Phys. Status Solidi B **252,** No. 5, 989–995 (2015) / **DOI** 10.1002/pssb.201451586

physica status solidi b
www.pss-b.com
basic solid state physics

Improved Ohmic contact to GaN and AlGaN/GaN two-dimensional electron gas using trap assisted tunneling by B implantation

Pankaj Upadhyay, Mudassar Meer, Kuldeep Takhar, Dolar Khachariya, Akhil Kumar S., Debashree Banerjee, Swaroop Ganguly, Apurba Laha, and Dipankar Saha

Department of Electrical Engineering, Applied Quantum Mechanics Laboratory, Centre of Excellence in Nanoelectronics, Indian Institute of Technology Bombay, Powai, Mumbai 400076, India

Received 30 September 2014, revised 14 February 2015, accepted 6 March 2015
Published online 23 March 2015

Keywords GaN, high electron mobility transistors, Ohmic contacts, trap assisted tunneling, two-dimensional electron gas

* Corresponding author: e-mail dipankarsaha@iitb.ac.in, Phone: +91-22-2576-7443, Fax: +91-22-25723707

We have demonstrated that deep level traps created by B implantation can reduce the contact resistance by forming an additional path for electron transport via trap assisted tunneling in GaN and AlGaN/GaN heterostructures. B implantation by plasma-immersion ion implantation creates deep level traps 0.36 eV below the conduction band edge to a shallow depth (10–25 nm) in the structure. These traps act as efficient percolation path for electrons between the TiN Ohmic contact and the active region, which can be bulk GaN or a two-dimensional electron gas (2DEG) formed at the AlGaN/GaN heterostructure. The improved Ohmic behavior is manifested as reduced specific contact resistivity and normalized contact resistance. The specific contact resistance and the normalized contact resistance are found to decrease by 59% (30%) and 86% (51%), respectively, for bulk GaN (AlGaN/GaN). The effect of B implantation on the sheet resistance of the 2DEG is insignificant when the implantation energy and post-implantation annealing time are controlled optimally.

1 Introduction GaN-based materials and devices are considered to be one of the most promising candidates for high power and radio frequency (RF) applications [1, 2]. GaN-based heterostructures have been found suitable for both electronic and optoelectronic devices [3, 4]. Low resistance Ohmic contact is an integral part for any device and a lot of efforts are being directed to improve the characteristics of the Ohmic contacts to GaN and related heterostructures. Ti/Al/Ni/Au is the most popular metal stack used for the Ohmic contact [5–7]. Other variants of metal stacks including Ti/Al/Mo/Au, Mo/Al/Mo/Au, and Ti/Al/Au are also being explored for low resistance contacts [8–10]. Non-alloyed Ohmic contact using Cr/Au is being explored for specific applications [10]. Efforts are also being directed to improve the surface condition for Ohmic contact formation by pre-processing techniques including BCl_3 treatment [12]. Si implanted processes are also in use to make the GaN heavily n-type before the formation of Ohmic contacts [13–15]. It is generally understood that the dominant mechanism for electron transport is tunneling between TiN and heavily doped GaN formed due to nitrogen vacancy [5, 16, 17]. Here, we have shown that intentional traps created by a boron (B) implantation can significantly reduce the contact resistance for GaN-based heterostructures. We have used Si-doped bulk GaN and AlGaN/GaN heterostructure containing 2DEG), which is prevalently used for high electron mobility transistors [1]. The B implantation creates deep traps, which form a parallel conduction path for electrons and reduce the contact resistance.

2 Device preparation Figure 1(a) and (b) shows the schematics of the GaN structures used in our study. The samples are grown by metalorganic chemical vapor deposition (MOCVD) technique. The bulk GaN sample [Fig. 1(a)] is subjected to B implantation from diborane by using plasma-immersion ion implantation (PIII). The process conditions are tabulated in Table 1. The sample

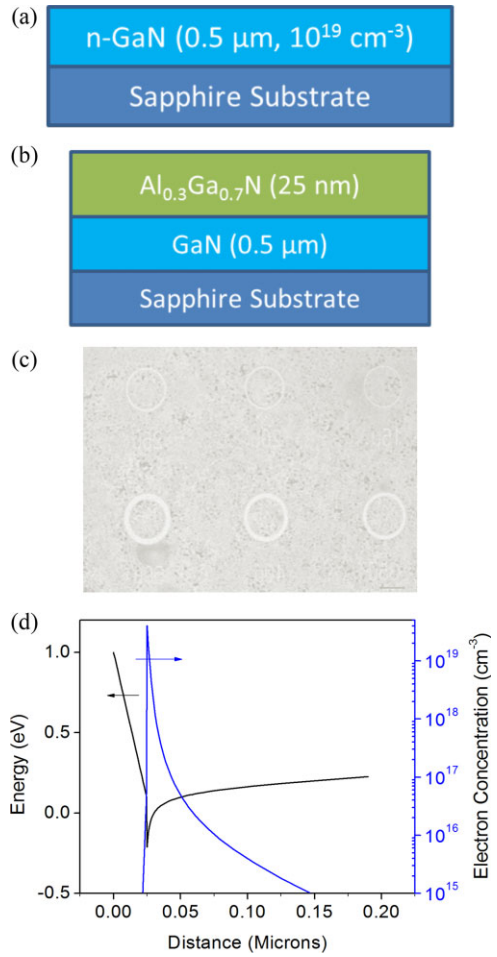

Figure 1 Schematic of (a) Si-doped bulk GaN and (b) AlGaN/GaN heterostructure for HEMT devices; (c) micro-photograph of the fabricated CTLM geometry. (d) Simulated band diagram and electron density plot showing that a two-dimensional electron gas (2DEG) is formed at the AlGaN/GaN interface. Efficient tunneling between the contact and 2DEG is a pre-requisite for low resistance Ohmic behavior.

is then annealed in a rapid thermal processing (RTP) chamber for 45 and 90 s at 825 °C in N_2 environment. We have used standard lithography techniques to delineate Ohmic contacts on as-grown samples (sample A) and on B implanted samples annealed for 45 s (sample B) and 90 s (sample C). Additional samples are also prepared with the B implant only in the contact region (sample D) to decouple the effect of sheet resistance and specific contact resistance on the overall contact resistance. The samples are cleaned using dilute HCl to remove native oxide before the deposition of the metal stack Ti/Al/Ni/Au (10/40/10/100 nm) by electron-beam evaporation under high vacuum (5×10^{-7} Torr). The samples are then annealed at 825 °C for 30 s to form the Ohmic contacts. The contacts are fabricated in the form of circular transmission line model (CTLM) geometry to determine the contact resistance (R_c), specific contact resistance (ρ_c), and sheet resistance (ρ_{sh}). The radius

Table 1 Process condition for plasma-immersion ion implantation.

process parameters	values
gas	diborane (5%) + He (95%)
gas pressure	20 sccm
power	1000 kW
process pressure	90 m Torr
ion density	10^9 cm^{-3}
frequency	4 kHz
pulse width	20 μs
implantation time	40 s
bias voltage	2 kV
current	35 mA

of the center contact is kept at 50 μm with separations as 15, 20, 25, 30, 35, 40, and 50 μm. Figure 1(c) shows a microphotograph of the fabricated device.

Experiments are also carried out to extend the same principle for GaN-based heterostructures particularly for 2DEG, which is used for high electron mobility transistors (HEMTs) [Fig. 1(b)]. The mobility and 2DEG electron density as determined from Hall measurements are found to be 6.6×10^{12} and 1900 cm^2/Vs, respectively. A typical simulated band diagram and electron density plot for 2DEG are shown in Fig. 1(d). Control devices are fabricated without B implant (sample E) to compare their characteristics with the B implanted samples. For implanted devices, the contact regions are only implanted with B before putting the Ohmic contacts. These implants are done at a lower bias (1 kV) to make sure that B does not reach AlGaN/GaN interface and a shallow profile is created. The B implanted samples are annealed for 45 s (sample F) and 90 s (sample G) at 825 °C in a RTP chamber. The B concentration as a function of depth for bulk GaN and AlGaN/GaN heterostructure as determined from secondary ion mass spectroscopy (SIMS) are shown in Fig. 2(a) and (b),

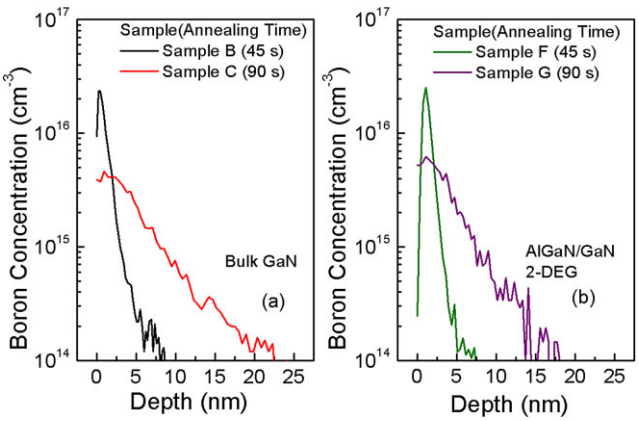

Figure 2 Boron depth profile for 45 s and 90 s annealed (a) bulk GaN and (b) AlGaN/GaN heterostructure samples. The penetration depth increases with increasing annealing time. A total of 90 s annealing leads to B very near to the two-dimensional electron gas in sample G leading to degraded sheet resistance.

Table 2 Details of the various bulk GaN and AlGaN/GaN heterostructure samples used in this study.

sample name	material	B implanted	bias voltage (kV)	annealing time (s)	channel implanted	Heterostructure
						Ohmic contact n-GaN Sapphire $Al_{0.3}Ga_{0.7}N$ B-implantation
A	GaN	No	–	–	–	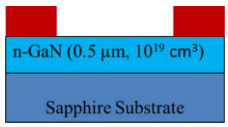
B	GaN	Yes	2	45	Yes	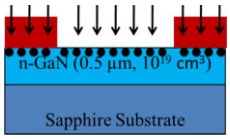
C	GaN	Yes	2	90	Yes	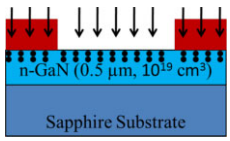
D	GaN	Yes	2	90	No	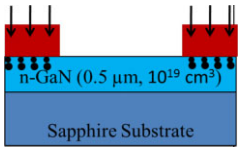
E	AlGaN/GaN	No	–	–	–	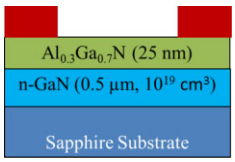
F	AlGaN/GaN	Yes	1	45	No	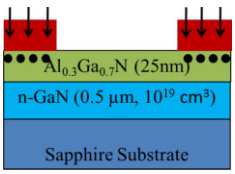
G	AlGaN/GaN	Yes	1	90	No	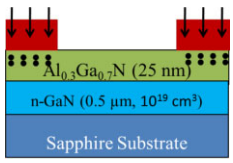
H (Schottky)	GaN	Yes	1	45	No	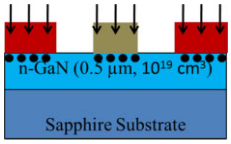

respectively. It may be noted that B penetrates more with increasing annealing time and the peak concentration decreases at the surface. B reaches very close to 2DEG for 90 s annealing time (sample G). The Ohmic contacts are made on these samples in CTLM geometry using the same techniques mentioned earlier. We have also fabricated Schottky diodes with 500 μm (sample H) on 45 s annealed B implanted samples with Ni/Au (20/100 nm) as the central contact. The details of all the devices are listed in Table 2. Temperature-dependent electrical measurements are carried out in a Lakeshore cryogenic probe station using Keithley source-measuring units.

3 Effect of the B implant To determine the effect of B implant on GaN and subsequent annealing, temperature-dependent photoluminescence (PL) measurements are carried out for the GaN samples. Figure 3(a) and (b) shows the temperature-dependent PL for sample A and sample B, respectively. It may be noted that the maximum intensity is observed for the as-grown sample at 3.4 eV (GaN band-gap at 300 K) and it reduces for the B implanted sample B. The shift in the PL peak position is due to reduction in band-gap with decreasing temperature. The B implanted samples show a broader yellow emission between 1.55 and 1.65 eV relative to the respective peak intensities. The enhanced yellow emission is a signature of deep level traps in GaN. Some of the electron–hole pairs recombine through the sub-band gap traps leading to long wavelength emission in the yellow band. This indicates near mid-gap traps are created by the B species. The activation energy for the primary peak is determined using the Arrhenius relation and Fig. 3(c)

$$I = I_0/[1 + A\exp(-E_{a1}/kT) + B\exp(-E_{a2}/kT)], \quad (1)$$

where I_0 is the intensity at low temperature, E_{a1} and E_{a2} are the thermal activation energies at high- and low-temperature regions, respectively, and A and B measure the strengths of both quenching processes. E_{a1} is found to be 3.2 and 0.017 meV for as-grown (sample A) and 45 s annealed (sample B) samples, respectively. A decreasing value of activation energy at higher temperature for B implanted samples indicates low efficiency of luminescence due to additional traps created by B. X-ray diffraction (XRD) studies are also carried out on these samples. Figure 3(d) shows the XRD characteristics for various bulk GaN samples. The fundamental characteristics do not change due to B implant and subsequent annealing. There is a slight reduction in full width at half-maximum (FWHM) due to annealing. The XRD characteristics for the AlGaN/GaN heterostructure samples are shown in Fig. 3(e). Similar trend is observed as that of bulk GaN samples.

The temperature-dependent I–V characteristics of all the samples are determined for a DC voltage swing of −3 to +3 V. A least-square linear fit is done to determine the contact resistance as a function of various separations in the CTLM geometry. All the samples show ideal linear characteristics with the Pearson product (regression coefficient) 0.995 or better. The B implanted 90 s annealed sample C shows the minimum resistance and as-grown samples show maximum resistance. The total contact resistance is determined by the specific contact resistance and sheet resistance. It may be noted that the processes required to reduce specific contact resistivity may have inadvertent effect on the sheet resistance and therefore we have determined both the parameters and observed their impact on the contact resistance. Figure 3(a) shows the resistance (after correction due to CTLM geometry)

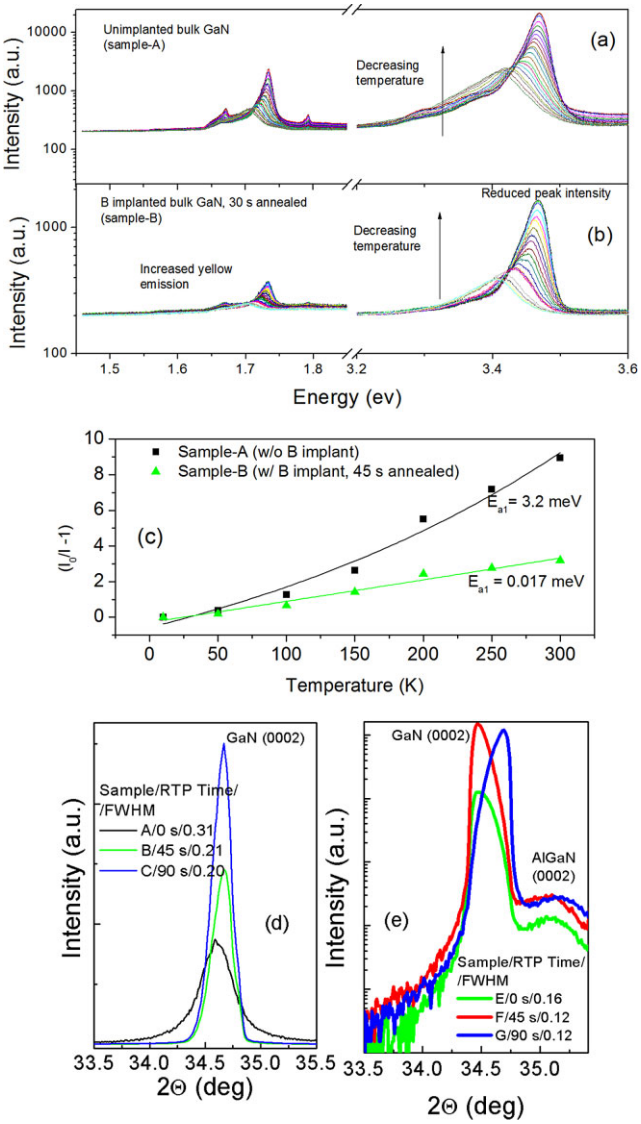

Figure 3 Temperature-dependent photoluminescence for (a) bulk GaN and (b) B implanted GaN annealed for 45 s. The peak intensity reduces significantly due to B implantation. A broad yellow emission is observed for B implanted samples. (c) Arrhenius plot for integrated PL intensity. High temperature activation energy is very small for B implanted sample (sample B) due to traps. (d,e) XRD characteristics for B implanted and post-annealed samples A–C on bulk GaN and samples E–G on AlGaN/GaN, respectively.

as a function of separation at 300 K. The correction factors are tabulated in the inset of Fig. 4(a). The minimum value for ρ_c is found to be for sample C (3.5 $\mu\Omega\,cm^2$); sample A shows a maximum value of 25.6 $\mu\Omega\,cm^2$, while that of sample B (8.3 $\mu\Omega\,cm^2$) lies in between at 300 K. The contact resistances ($R_c/2\pi R$) and transfer lengths (L_T) for various samples are shown in Fig. 4(b). The contact resistance and transfer length are determined by extrapolating the lines and finding the intercepts with y-axis ($2R_c$) and x-axis ($2L_T$), respectively. It may be noted that the decreases in contact resistance are associated with a decrease in transfer length. The sheet resistance ρ_{sh} is also determined for all the cases. Figure 4(c) shows ρ_c and ρ_{sh} for samples A, B, and C. It may be noted that ρ_{sh} increases monotonically with increasing B implant annealing time, whereas ρ_c decreases with increasing annealing time. The sheet resistances for samples A, B, and C are found to be 573, 633, and 747 Ω/□. The characterizations are also done as a function of temperature to determine the temperature sensitivity for both ρ_c and ρ_{sh}. Figure 5(a) and (b) shows ρ_c and ρ_{sh} as a function of temperature, respectively. It may be noted that ρ_c is relatively insensitive to temperature and it decreases slightly with increasing temperature for B implanted samples [Fig. 5(a)]. ρ_c changes from 42.2 to 25.6 $\mu\Omega\,cm^2$ and 4.1 to 3.5 $\mu\Omega\,cm^2$ for as-grown (sample A) and B implanted sample C, respectively. Control measurements are also done where only the contact

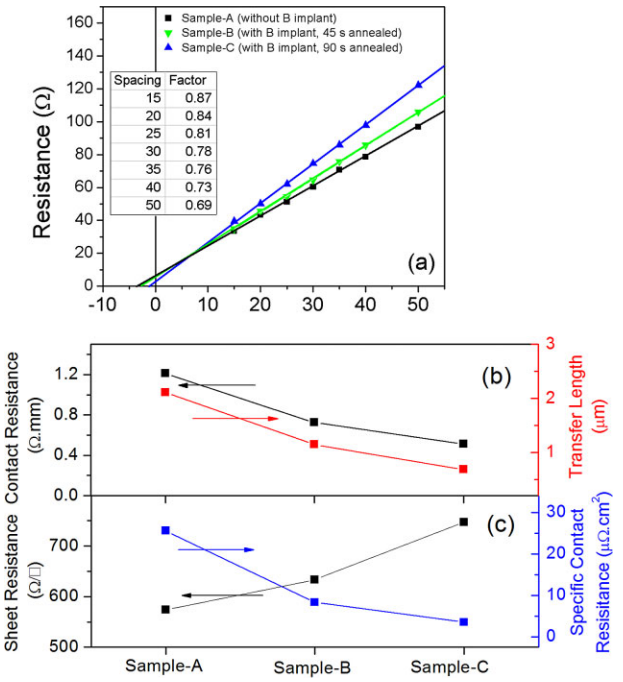

Figure 4 (a) Resistance versus separation for as-grown and B implanted (annealed for 45 s and 90 s) samples. The resistance decreases for B implanted samples. (b) Contact resistance and transfer length, (c) sheet resistance and specific contact resistance plotted for as-grown and B implanted samples. The specific contact resistance decreases, however, sheet resistance increases due to B implant.

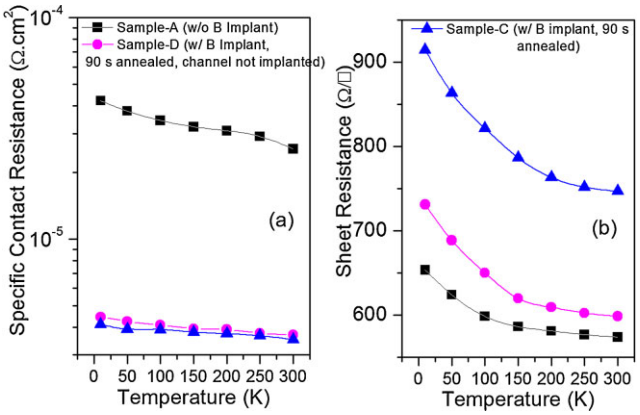

Figure 5 (a) Specific contact resistance and (b) sheet resistance as a function of temperature for as-grown and B implanted samples. The specific contact resistance for B implanted sample is relatively independent of temperature as tunneling is the dominant mechanism for electron transport. Sheet resistance reduces with increasing temperature due to increased ionization of Si dopants at higher temperature.

regions are implanted with B (sample D). They show similar values for ρ_c as that of sample C. However, ρ_{sh} shows very strong temperature dependence [Fig. 5(b)]. The decrease in sheet resistance for increasing temperature may be understood from the ionization of dopants at higher temperatures. Sheet resistance increases significantly for B implantation with the minimum sheet resistance (573 Ω/□ at 300 K) is observed for as-grown samples. It may be noted that the sheet resistance shows a lesser degree of degradation where the channel is protected from B implantation.

The observed phenomena can be explained by considering the electron transport for the Ohmic contacts. The potential mechanism has been proposed to be the formation of TiN film during the annealing of metal stack on GaN-based materials and creating large number of N vacancies, which make the material heavily n-type doped [5]. The equivalent doping concentration can be very large ($\sim 10^{20}\,cm^{-3}$) for a few nanometers of TiN. The electrons then tunnel efficiently from TiN to GaN leading to the Ohmic contact formation. Similar mechanism has been found responsible for Ohmic contacts to 2DEG system for AlGaN/GaN heterostructures as well, where the Ohmic contact formation is explained by the formation of TiN contact inclusions (CIs), followed by tunneling due to field emission and thermionic field emission under bias [16, 17]. It is therefore imperative that additional tunneling mechanism should reduce the contact resistance further. Deep traps are added in the barrier layer between TiN and GaN due to B. An increase in the annealing time leads to an increased penetration of traps into GaN and more number of traps are expected to be electrically active. The traps create additional paths for electron tunneling between TiN and GaN. This additional conduction path reduces ρ_c. Since the tunneling current is relatively independent of

temperature, the decrease of the temperature dependence of tunneling current with annealing for B implanted samples [Figs. 5(a) and 6(a)] further corroborates our observations. It is experimentally observed that ρ_{sh} is higher for B implanted samples and it increases with increasing annealing time. The additional traps created by the B implant within the channel region reduce the mobility of electrons, which lead to an increase in ρ_{sh}. Further increase in ρ_{sh} with increasing annealing time is due to the degradation of mobility over a larger depth of GaN. However, the change in ρ_{sh} for samples where B implantation is done only for the source and drain regions (sample D) is relatively small as the mobility degradation only affects the transport beneath the contact regions.

Electrical characterizations are also carried out for CTLM devices on AlGaN/GaN heterostructure (samples E–G). Figure 6(a), (b), and (c) shows ρ_c, ρ_{sh}, and R_c for these devices as determined from the variation of resistance as a function of separation, respectively. It is observed that ρ_c decreases for B implanted samples annealed for less time (45 s) from 59.7 (sample E) to 2.8 $\mu\Omega\,cm^2$ (sample F). No noticeable change for ρ_{sh} ($\sim$500 $\Omega/\square$) is observed due to B implant and subsequent annealing. This confirms that trap assisted tunneling is effective in reducing contact resistance in these heterostructures. No significant change in ρ_c is observed with temperature as tunneling is the dominant mechanism for electron transport. The ρ_c is found to be very large (1.3 $m\Omega\,cm^2$) for 90 s annealed samples (sample G). The observed phenomena may be explained from the fact that larger annealing time leads to increased penetration of B into the heterostructure and deteriorating 2DEG mobility and carrier concentration. This is further confirmed through control measurements with B implant at 2 kV bias. The resistance increases by four orders of magnitude for the same separation in CTLM geometry. Figure 6(b) shows ρ_{sh} as a function of temperature. It decreases with increasing temperature because of increased phonon scattering and mobility reduction. It may be noted that the ρ_{sh} does not degrade for B implantation (sample G) under optimum condition. The reduction of contact resistance as a function of temperature is shown in Fig. 6(c).

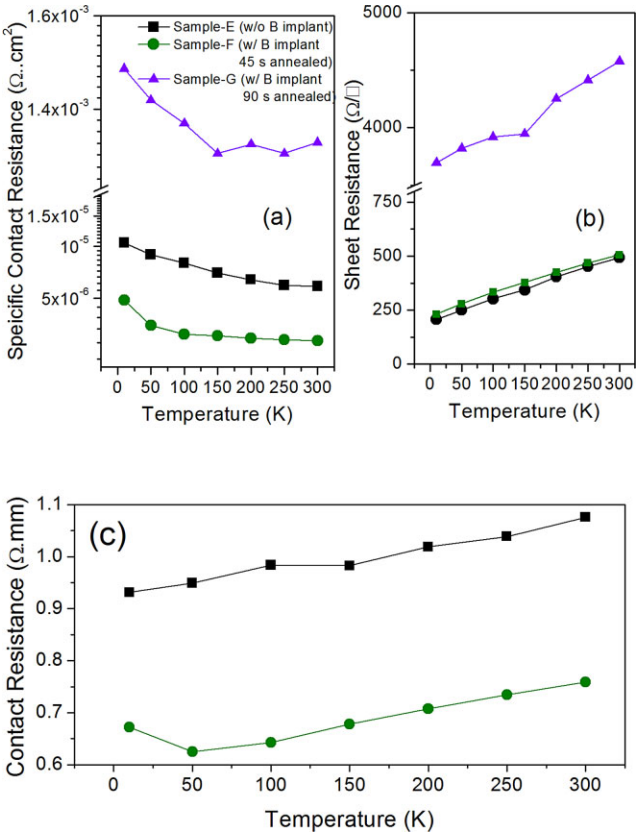

Figure 6 (a) Specific contact resistance, (b) sheet resistance, and (c) contact resistance as a function of temperature for as-grown and B implanted AlGaN/GaN heterostructures. The specific contact resistance reduces due to trap assisted tunneling. The B impurities in the channel region critically reduce the 2DEG conductance. The sheet resistance increases with temperature due to increased phonon scattering and reduced mobility.

Schottky diodes are also fabricated on B implanted bulk GaN (sample H) to electrically determine the trap level. The current–voltage characteristics on these devices with Ni/Au (20/100 nm) as the Schottky contact and the conventional Ti/Al/Ni/Au as the Ohmic contact show linear behavior instead of rectifying nature, indicating that trap assisted tunneling is very efficient in creating a percolation path for electrons. This prevents direct capacitance–voltage measurements on these devices. We have fabricated additional Schottky diodes with lower concentration for B, which preserves the rectifying nature. Deep-level transient spectroscopy (DLTS) is carried out on these samples along with the unimplanted sample to identify the defect energy level (Fig. 7). The Arrhenius plot is shown in the inset of Fig. 7. It is observed that B implantation introduces an additional trap level at 0.36 eV below conduction band edge in addition to the existing trap levels at 0.25, 0.57, and 0.90 eV in the bulk material.

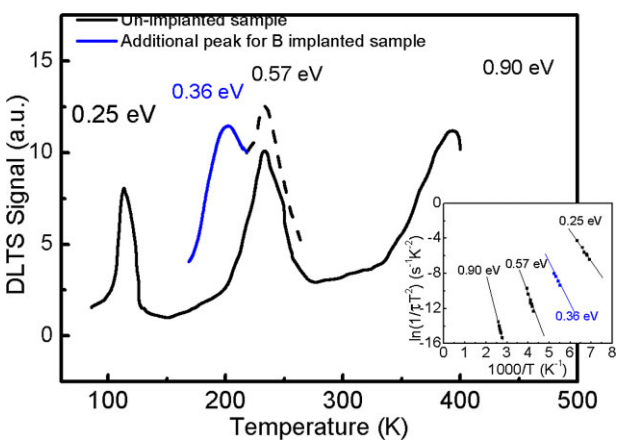

Figure 7 DLTS characteristics for un-implanted and B implanted samples. B gives rise to a new trap level at 0.36 eV below the conduction band edge. The Arrhenius plot is shown in the inset.

4 Conclusions In summary, we have demonstrated that the contact resistance to n-GaN and 2DEG in AlGaN/GaN heterostructures can be significantly reduced by using trap assisted tunneling. The traps are intentionally created by B implantation. PL study indicates that the traps are mostly located in the mid-gap region. The specific contact resistance reduces substantially without degrading the sheet resistance significantly. The Ohmic performance improvement for AlGaN/GaN heterostructure can yield better RF performance for HEMTs. The same fundamental principle of trap assisted tunneling for contact resistance reduction can be extended to other Ohmic metal stacks as well.

Acknowledgements This work is partially supported by Department of Science and Technology under grant no. SR/S3/EECE/0186/2012. We thank SAIF IIT Bombay for physical characterization.

References

[1] U. K. Mishra, P. Parikh, and Y. Wu, Proc. IEEE **90**, 1022 (2002).
[2] J. Edmond, A. Abare, M. Bergman, J. Bharathan, K. L. Bunker, D. Emerson, K. Haberern, J. Ibbetson, M. Leung, P. Russel, and D. Slater, J. Cryst. Growth **272**, 242 (2004).
[3] S. Nakamura, T. Mukai, and M. Senoh, Appl. Phys. Lett. **64**, 1687 (1994).
[4] S. D. Lester, F. A. Ponce, M. G. Craford, and D. A. Steigerwald, Appl. Phys. Lett. **66**, 1259 (1995).
[5] M. E. Lin, Z. Ma, F. Y. Huang, Z. F. Fan, L. H. Allen, and H. Morkoc, Appl. Phys. Lett. **64**, 1004 (1994).
[6] F. A. Faria, J. Gui, P. Zhao, G. Li, P. K. Kandaswamy, M. Wistey, H. Xing, and D. Jena, Appl. Phys. Lett. **101**, 032109 (2012).
[7] S.-H. Lim, J. Washburn, Z. Liliental-Weber, and D. Qiao, Appl. Phys. Lett. **78**, 3797 (2001).
[8] D. Selvanathan, F. M. Mohammed, A. Tesfayesus, and I. Adesida, J. Vac. Sci. Technol B **22**, 2409 (2004).
[9] Z. X. Qin, Z. Z. Chen, Y. Z. Tong, X. M. Ding, X. D. Hu, T. J. Yu, and G. Y. Zhang, Appl. Phys. A **78**, 729 (2004).
[10] S. Ruvimuv, Z. Liliental-Weber, J. Washburn, K. J. Duxstad, E. E. Haller, Z.-F. Fan, S. N. Mohammad, W. Kim, A. E. Botchkarev, and H. Morkoc, Appl. Phys. Lett. **69**, 1556 (1996).
[11] M. Lee, J. Sheu, and C. C. Hu, Appl. Phys. Lett. **91**, 182106 (2007).
[12] T. Fujishima, S. Joglekar, D. Piedra, H.-S. Lee, Y Zhang, A. Uedono, and T. Palacios, Appl. Phys. Lett. **103**, 083508 (2013).
[13] J. K. Sheu, C. J. Tun, M. S. Tsai, C. C. Lee, G. C. Chi, S. J. Chang, and Y. K. Su, J. Appl. Phys. **91**, 1845 (2002).
[14] C. Nguyen, P. Shah, E. Leong, M. Derenge, and K. Jones, Solid State Electron. **54**, 1227 (2010).
[15] M. L. Lee, J. K. Sheu, L. S. Yeh, M. S. Tsai, C. J. Kao, C. J. Tun, S. J. Chang, and G. C. Chi, Solid State Electron. **12**, 2179 (2002).
[16] S. Kim, J.-H Ryou, R. D. Dupis, and H. Kim, Appl. Phys. Lett. **102**, 052107 (2013).
[17] M. Hajłasz, J. J. T. M. Donkers, S. J. Sque, S. B. S. Heil, D. J. Gravesteijn, F. J. R. Rietveld, and J. Schmitz, Appl. Phys. Lett. **104**, 242109 (2014).